Role of C. elegans TAT-1 Protein in Maintaining Plasma Membrane Phosphatidylserine Asymmetry

Monica Darland-Ransom, *et al.*

Science **320**, 528 (2008);
DOI: 10.1126/science.1155847

Science (print ISSN 0036-8075; online ISSN 1095-9203) is published weekly, except the last week in December, by the American Association for the Advancement of Science, 1200 New York Avenue NW, Washington, DC 20005.

Role of *C. elegans* TAT-1 Protein in Maintaining Plasma Membrane Phosphatidylserine Asymmetry

Monica Darland-Ransom,[1] Xiaochen Wang,[1]* Chun-Ling Sun,[1]* James Mapes,[1] Keiko Gengyo-Ando,[2] Shohei Mitani,[2] Ding Xue[1]†

The asymmetrical distribution of phospholipids on the plasma membrane is critical for maintaining cell integrity and physiology and for regulating intracellular signaling and important cellular events such as clearance of apoptotic cells. How phospholipid asymmetry is established and maintained is not fully understood. We report that the *Caenorhabditis elegans* P-type adenosine triphosphatase homolog, TAT-1, is critical for maintaining cell surface asymmetry of phosphatidylserine (PS). In animals deficient in *tat-1*, PS is abnormally exposed on the cell surface, and normally living cells are randomly lost through a mechanism dependent on PSR-1, a PS-recognizing phagocyte receptor, and CED-1, which contributes to recognition and engulfment of apoptotic cells. Thus, *tat-1* appears to function in preventing appearance of PS in the outer leaflet of plasma membrane, and ectopic exposure of PS on the cell surface may result in removal of living cells by neighboring phagocytes.

Class IV P-type adenosine triphosphatases (ATPases) are putative aminophospholipid translocases (APLTs) that are suggested to promote the inward movement of aminophospholipids such as phosphatidylserine (PS), resulting in the restriction of PS to the inner leaflet of the plasma membrane (*1*–*3*). There are six *Caenorhabditis elegans* homologs of the human aminophospholipid translocases (fig. S1A) (*4*), which were named the *tat* genes as transbilayer amphipath transporters. To investigate the functions of these *C. elegans tat* genes, we used the RNA interference (RNAi) method to reduce their expression and examined whether RNAi treatment of the *tat* genes altered PS distribution in *C. elegans* germ cells with an annexin V–based staining protocol that specifically labels surface-exposed PS in *C. elegans* germ cells (*5*).

In wild-type *C. elegans*, no PS staining was observed on the surface of normal germ cells (Fig. 1A), whereas about 60% of apoptotic germ cells were labeled by annexin V (*5*). In *tat-1*(RNAi)–treated animals, PS staining was observed on the surface of many normal germ cells (Fig. 1B). These PS-stained germ cells appeared not to be

[1]Department of Molecular, Cellular, and Developmental Biology, University of Colorado, Boulder, CO 80309, USA. [2]Department of Physiology, Tokyo Women's Medical University School of Medicine and Core Research for Embryonic Science and Technology (CREST), Japan Science and Technology Agency (JST), Tokyo, 162-8666, Japan.

*These authors contribute equally to this work.
†To whom correspondence should be addressed. E-mail: ding.xue@colorado.edu

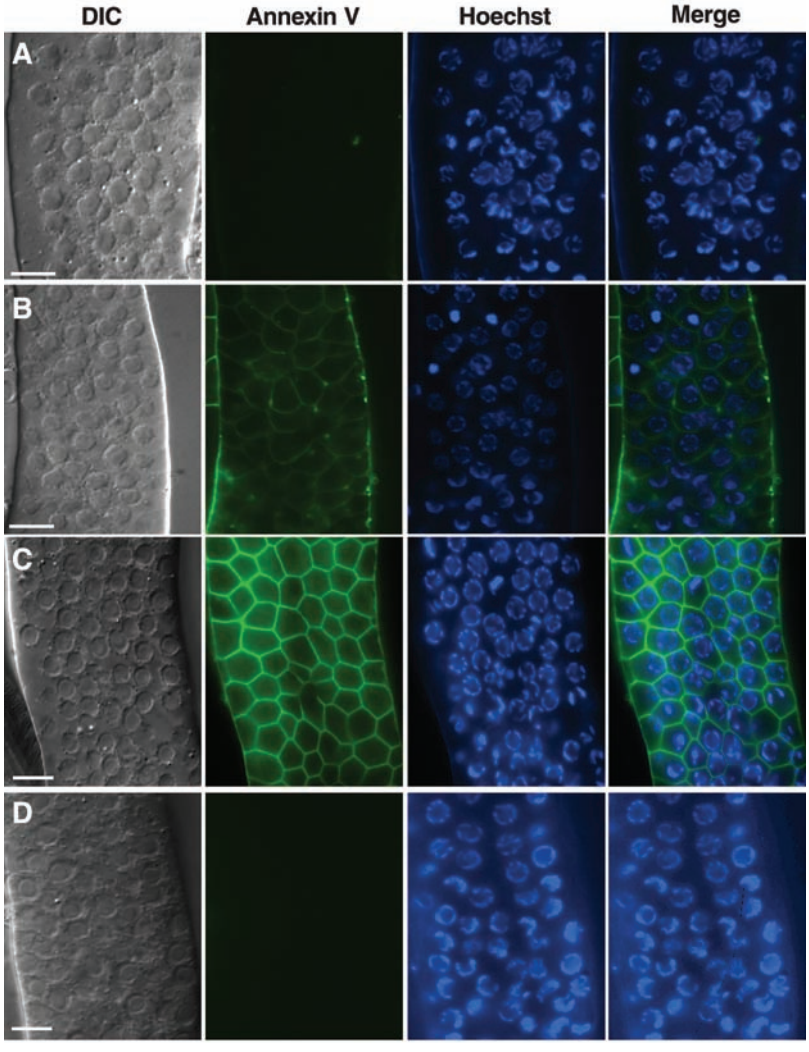

Fig. 1. Exposure of PS on the surface of *C. elegans* germ cells in *tat-1*–deficient animals. Exposed gonads of the following hermaphrodite adult animals were stained with annexin V (*5*): (**A**) wild-type animal (N2), (**B**) *tat-1* RNAi-treated N2 animal, (**C**) *tat-1(tm1034)* animal, and (**D**) *tat-3(tm1275)* animal. Images of differential contrast interference (DIC), annexin V staining, Hoechst 33342 staining, and the merged image of annexin V plus Hoechst 33342 staining are shown. Scale bars indicate 6.5 μm.

apoptotic cells or damaged cells because they lacked the raised buttonlike morphology and the condensed Hoechst 33342 DNA staining pattern that are characteristic of apoptotic germ cells and were not stained by propidium iodide, which stains necrotic or damaged cells (*6*, *7*). RNAi of the other *tat* genes (*tat-2*, *tat-3*, *tat-4*, *tat-5*, and *tat-6*) did not result in PS staining on the surface of living germ cells (table S1). Thus, reduction of the *tat-1* activity alone appears to be sufficient to disrupt asymmetrical PS distribution on the surface of *C. elegans* germ cells.

To confirm the RNAi results, we isolated a deletion allele of *tat-1* (*tm1034*) and a deletion allele of *tat-3* (*tm1275*) (*4*). The *tat-1(tm1034)* mutant contains a 597–base pair (bp) deletion plus a 1-bp insertion in the *tat-1* locus that is predicted to cause a frame shift and an early stop after exon five (fig. S1B) and would remove the ATPase domain as well as 8 of the 10 putative transmembrane domains of TAT-1. The *tat-3(tm1275)* mutant has a 446-bp deletion and a 7-bp insertion that removes parts of the first two exons of the *tat-3* gene and is likely a null allele (fig. S1B).

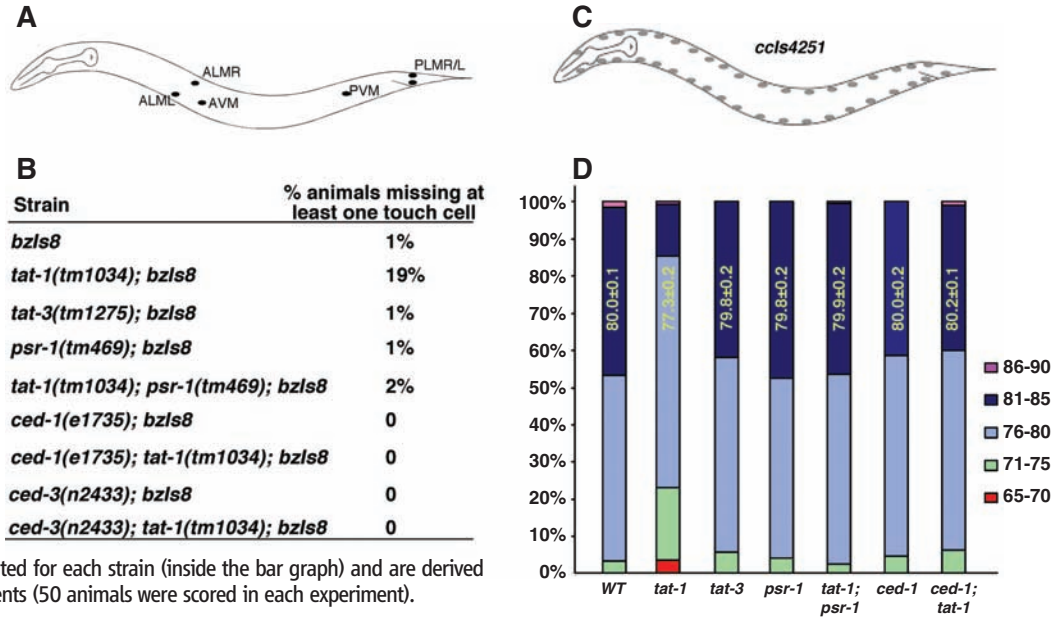

Fig. 2. Random loss of neurons and muscle cells in *tat-1*–deficient animals through a mechanism mediated by *psr-1* and *ced-1*. An integrated GFP reporter line, *bzIs8*, labels six touch-receptor neurons and an integrated GFP reporter line, *ccIs4251*, directs GFP expression in body-wall muscle cells. Neurons or muscle cells that were scored are indicated with black or gray circles (**A** and **C**). The presence of neurons or the number of muscle cells was scored by using a Nomarski microscope with epifluorescence. The percentages of animals missing one or more neurons (**B**) or the percentages of animals with a certain range of muscle cell numbers (**D**) are shown. At least 200 animals were scored for each strain. The average muscle cell number and standard error of mean (SEM) are indicated for each strain (inside the bar graph) and are derived from at least four independent experiments (50 animals were scored in each experiment).

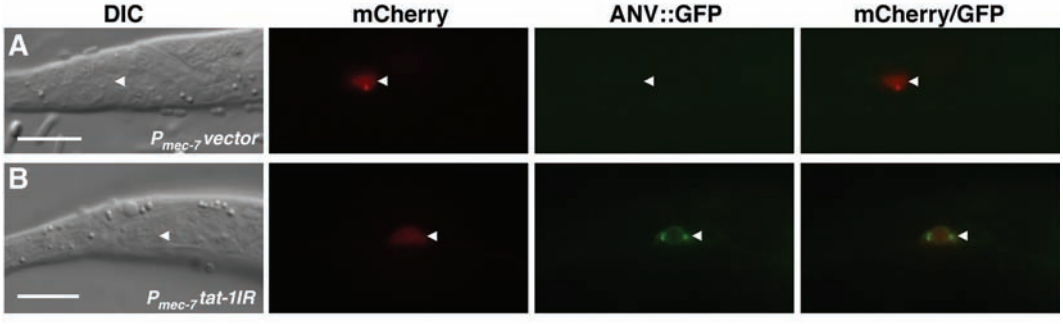

C

Strain	% PLM cells showing surface ANV::GFP
P_{mec-7} vector, L1	10% (64)
P_{mec-7} vector, L2	10% (64)
P_{mec-7} vector, L3	5% (64)
P_{mec-7}*tat-1IR*, L1	50% (65)
P_{mec-7}*tat-1IR*, L2	57% (64)
P_{mec-7}*tat-1IR*, L3	60% (51)

D

Strain	% PLM cell missing
P_{mec-7} vector, L1	4% (50)
P_{mec-7} vector, L2	4% (67)
P_{mec-7} vector, L3	3% (66)
P_{mec-7}*tat-1IR*, L1	13% (55)
P_{mec-7}*tat-1IR*, L2	15% (62)
P_{mec-7}*tat-1IR*, L3	19% (62)
ced-1(e1735); P_{mec-7}*tat-1IR*, L1	7% (60)
ced-1(e1735); P_{mec-7}*tat-1IR*, L2	4% (61)
ced-1(e1735); P_{mec-7}*tat-1IR*, L3	3% (60)
psr-1(tm469); P_{mec-7}*tat-1IR*, L1	4% (61)
psr-1(tm469); P_{mec-7}*tat-1IR*, L2	5% (60)
psr-1(tm469); P_{mec-7}*tat-1IR*, L3	7% (61)

Fig. 3. PS exposure on the surface of the PLM touch cells and PLM cell loss in animals with cell type–specific knockdown of the *tat-1* gene. Animals carrying an integrated transgene harboring P_{hsp}ANV::GFP and an extrachromosomal array containing P_{mec-4}mCherry and P_{mec-7}vector (**A**) or P_{mec-4}mCherry and P_{mec-7}*tat-1IR* (**B**) were subjected to heat-shock treatment at 30°C for 35 min. Two hours later, L2 transgenic larvae were examined with use of a Nomarski (Zeiss, Göttinger, Germany) microscope with epifluorescence. The presence of the PLM cell (indicated by an arrowhead) is revealed by the expression of monomeric Cherry protein (mCherry) from P_{mec-4}mCherry. PS exposure on the surface of the PLM cell is indicated by ANV::GFP labeling. [(A) and (B)] Images of DIC, mCherry, ANV::GFP, and the merged image of mCherry/ANV::GFP are shown. Scale bars indicate 10 μm. (**C**) Quantification of the percentage of the PLM cells showing surface-exposed PS. (**D**) Quantification of the percentage of the PLM cells lost. L1, L2, and L3 indicate three independent transgenic lines for each indicated construct (all contain P_{mec-4}mCherry). Animals carrying these arrays were then crossed into the *ced-1(e1735)* or the *psr-1(tm469)* mutant to generate the mutant strains carrying the same arrays. Numbers in parentheses indicate the number of animals scored. Each animal has two PLM cells (PLML and PLMR).

tat-1(tm1034) and *tat-3(tm1275)* animals are viable and superficially indistinguishable from each other. Both mutants display a low penetrance of lethality and dumpy (Dpy) phenotypes. *tat-1(tm1034)* animals also have increased numbers of spontaneous males.

When we stained exposed gonads of the *tat-1(tm1034)* and *tat-3(tm1275)* animals with annexin V, all germ cells in *tat-1(tm1034)* animals displayed strong PS staining on their surface (Fig. 1C). No germ cells from the *tat-3(tm1275)* animals were stained by annexin V (Fig. 1D). Germ cell staining for PS in *tat-1(tm1034)* animals was stronger and more widespread than that in *tat-1* RNAi animals (Fig. 1, B and D) and was not affected by loss of the *C. elegans* phospholipid scramblases (SOM text and fig. S2), some of which promotes PS externalization in apoptotic cells (*5*). Taken together, these results suggest that *tat-1* is essential for keeping PS from the outer leaflet of plasma membrane and provide in vivo evidence that a member of the aminophospholipid translocase family functions to restrict PS to the inner leaflet of the plasma membrane, possibly by promoting inward movement of PS from the outer leaflet.

A study using a fusion protein containing green fluorescent protein and annexin V (GFP::AnxV) as a PS sensor reached the opposite conclusion that *tat-1* promotes externalization of PS in *C. elegans* apoptotic cells (*8*). We think that the difference between the two studies could result from the relatively weak binding of GFP::AnxV in vivo to surface-exposed PS and a high-staining background (SOM text and fig. S3). The optimized ex vivo PS-staining protocol that we used generated strong and specific PS staining (fig. S3) (*5*), and we did not observe reduced PS staining of apoptotic germ cells in the *tat-1(tm1034)* mutant (SOM text and fig. S4), indicating that *tat-1* does not promote externalization of PS in apoptotic cells.

Because externalization of PS is a conserved event during apoptosis and has been proposed to serve as an engulfment signal to trigger phagocytosis of apoptotic cells (*5*, *9*, *10*), we examined whether loss of the *tat-1* activity affected apoptosis or removal of apoptotic cells in *C. elegans*. The *tat-1(tm1034)* mutation did not affect the numbers of embryonic cell corpses present in various embryonic stages in which most somatic cell deaths occur or the numbers of germ cell corpses in the germ line (fig. S5), suggesting that *tat-1* alone does not have a detectable role in apoptosis or removal of apoptotic cells. However, we observed that some cells were missing in the *tat-1(tm1034)* mutant and therefore used integrated transgenes carrying various GFP reporters that label specific cells or cell types to help identify the missing cells in the *tat-1* mutant. For example, the *bzIs8* transgene specifically labels six touch-receptor neurons (*11*). In *tat-1(tm1034); bzIs8* animals, all six touch cells were randomly lost in a certain percentage of animals (from 1% to 9% depending on the specific touch cells), and 19% of animals lost at least one touch-receptor neuron (Fig. 2, A and B). Touch-receptor neurons were rarely missing in *bzIs8* or *tat-3(tm1275); bzIs8* animals. A similar percentage of animals (24%) were missing at least one cell in *inIs179*; *tat-1(tm1034)* animals, in which 16 neurons were labeled by the $P_{ida\text{-}1}$*gfp* reporter (fig. S6, A and B) (*12*). Again, all neurons labeled by *inIs179* were randomly lost, and such cell loss was not seen in *inIs179* or *inIs179; tat-3(tm1275)* animals. The missing-cell phenotype of the *tat-1(tm1034)* mutant was not restricted to neurons; hypodermal, epithelial, and muscle cells were randomly lost as well. For example, wild-type animals contain an average of 80 body-wall muscle cells (labeled by the *ccIs4251* transgene) with a range from 71 to 90 muscle cells in individual animals (Fig. 2, C and D) (*13*). In *tat-1(tm1034)* animals, the average number of muscle cells was reduced to 77 ($P < 0.0001$, unpaired *t* test), ranging from 65 to 90 muscle cells, with 23% of animals containing less than 76 muscle cells and 15% of animals having more than 80 muscle cells. In comparison, only 3 to 6% of wild-type or *tat-3(tm1275)* animals have less than 76 muscle cells, and 43 to 47% of them have more than 80 muscle cells. Thus, loss of the *tat-1* activity but not loss of the *tat-3* activity causes indiscriminate cell loss in various cell types.

We then examined whether normal somatic cells also expose PS in the *tat-1(tm1034)* mutant. The ex vivo germ-cell PS-staining protocol cannot be applied to stain somatic cells, which are enclosed by a hard, impermeable eggshell. Expression of a secreted annexin V–GFP fusion similar to the one used by Zullig *et al.* (*8*) in the *tat-1(tm1034)* mutant did not reveal obvious surface PS exposure in normal somatic cells, possibly because of competition for binding to the annexin V–GFP fusion and high background staining. We therefore generated cell type–specific knockdown of the *tat-1* gene by expressing a *tat-1* inverted-repeat (IR) RNAi construct in six touch cells under the control of the *C. elegans mec-7* promoter ($P_{mec\text{-}7}$*tat-1IR*). This construct generates double-stranded RNA (dsRNA) that reduces gene expression in vivo (*14*). A high percentage of the posterior lateral microtubule (PLM) touch cells (50 to 60%) in transgenic animals carrying $P_{mec\text{-}7}$*tat-1IR* and expressing a secreted annexin V–GFP fusion under the control of heat-shock promoters (P_{hsp}ANV::GFP) displayed ANV::GFP on their surface (Fig. 3, B and C). In contrast, transgenic animals carrying a control vector and P_{hsp}ANV::GFP had a low percentage of PLM cells (5 to 10%) labeled by ANV::GFP, which may be nonspecific staining (Fig. 3, A and C). Furthermore, in transgenic animals carrying $P_{mec\text{-}7}$*tat-1IR*, 13 to 19% of the PLM neurons were missing, whereas in transgenic animals carrying the control vector few PLM neurons (3 to 4%) were lost (Fig. 3D). Together, these results demonstrate that reduction of *tat-1* activity may cause inappropriate PS exposure on the surface of somatic cells and the random loss of these cells.

We investigated the cause of random cell loss in the *tat-1(tm1034)* mutant. PS or oxidized PS exposed on the surface of apoptotic cells can act as a signal to trigger phagocytic removal of apoptotic cells (*5*, *9*, *15*, *16*). A loss-of-function mutation (*tm469*) in the *C. elegans psr-1* gene, which encodes a PS-binding phagocyte receptor (*5*, *17*), rescued the missing cell phenotype in the *tat-1* mutant and the $P_{mec\text{-}7}$*tat-1IR* animals (Figs. 2, B and D and 3D, and fig. S6B). *psr-1* has a minor role in *C. elegans* in removing apoptotic cells (*17*), which likely contain multiple engulfment signals, but appears to have a major role in the *tat-1* mutant to mediate removal of normal cells with surface-exposed PS. Similarly, a loss-of-function mutation (*e1735*) in the *ced-1* gene, which is important for recognition and engulfment of apoptotic cells (*18*), or a loss-of-function mutation (*n2433*) in *ced-3*, which encodes the key cell-killing caspase in *C. elegans* and cooperates with the phagocytosis process to kill cells (*19*–*21*), suppressed the missing cell phenotype of the *tat-1* mutant (Fig. 2, B and D, and fig. S6B). Thus, cells in the *tat-1* mutant are lost through a phagocytic mechanism that is used to remove apoptotic cells.

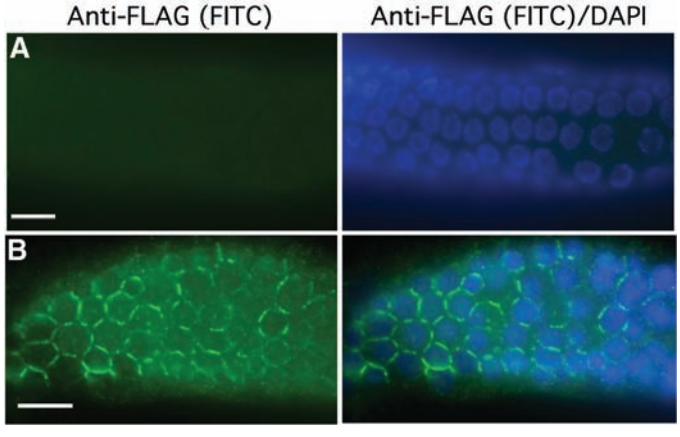

Fig. 4. Localization of TAT-1 to plasma membrane of *C. elegans* germ cells. Gonads from a *tat-1(tm1034); bzIs8* animal (**A**) and a *tat-1 (tm1034); smIs142; bzIs8* animal (**B**) were dissected out and stained with M2 monoclonal antibody (anti-FLAG) (*4*). *smIs142* is an integrated transgene carrying $P_{tat\text{-}1}$*tat-1::flag*. Images of *C. elegans* gonads with fluorescein isothiocyanate (FITC) staining (anti-FLAG) and FITC/4′,6′-diamidino-2-phenylindole (DAPI) staining are shown. The mosaic pattern of FITC staining in (B) may be due to partial germline silencing of the *smIs142* transgene (*25*). Scale bars indicate 6.5 μm.

We examined the cellular localization of TAT-1 by expressing a TAT-1 fusion protein tagged at its carboxyl terminus with a FLAG epitope under the control of the *tat-1* gene promoter ($P_{tat\text{-}1}$*tat-1::flag*). Several extrachromosomal transgene arrays and an integrated transgene (*smIs142*) carrying $P_{tat\text{-}1}$*tat-1::flag* were generated and all fully rescued the missing cell phenotype of the *tat-1(tm1034)* mutant (table S2). *smIs142* also partially rescued the germ cell PS exposure defect of the *tat-1(tm1034)* mutant (fig. S7). Immunostaining of gonads from the *smIs142* animals using a monoclonal antibody (M2) to the FLAG epitope revealed that TAT-1 localizes predominantly on the plasma membrane (Fig. 4).

Class IV P-type ATPases have been suggested to promote translocation of aminophospholipids [PS and phosphatidylethanolamine (PE)] from the outer leaflet to the inner leaflet of plasma membrane and thus may have a role in maintaining asymmetrical distribution of PS and PE on the lipid bilayer (*3*, *22*, *23*). However, in multicellular organisms, multiple members of this ATPase family exist (at least 14 were identified in mammals), which prevents genetic analysis of their in vivo functions (*3*, *22*, *24*). Our findings thus provide important in vivo evidence that a member of the aminophospholipid translocase family is involved in maintaining PS asymmetry on plasma membrane and that disruption of such PS asymmetry can result in indiscriminate removal of affected cells by neighboring phagocytes.

References and Notes

1. M. E. Auland, B. D. Roufogalis, P. F. Devaux, A. Zachowski, *Proc. Natl. Acad. Sci. U.S.A.* **91**, 10938 (1994).
2. J. K. Paterson *et al.*, *Biochemistry* **45**, 5367 (2006).
3. D. L. Daleke, *J. Lipid Res.* **44**, 233 (2003).
4. Materials and methods are available on *Science* Online.
5. X. Wang *et al.*, *Nat. Cell Biol.* **9**, 541 (2007).
6. Z. Darzynkiewicz *et al.*, *Cytometry* **13**, 795 (1992).
7. R. A. Harrison, S. E. Vickers, *J. Reprod. Fertil.* **88**, 343 (1990).
8. S. Zullig *et al.*, *Curr. Biol.* **17**, 994 (2007).
9. V. A. Fadok *et al.*, *J. Immunol.* **149**, 4029 (1992).
10. V. A. Fadok, D. Xue, P. Henson, *Cell Death Differ.* **8**, 582 (2001).
11. D. C. Royal *et al.*, *J. Biol. Chem.* **280**, 41976 (2005).
12. T. R. Zahn, M. A. Macmorris, W. Dong, R. Day, J. C. Hutton, *J. Comp. Neurol.* **429**, 127 (2001).
13. L. Timmons, D. L. Court, A. Fire, *Gene* **263**, 103 (2001).
14. N. Tavernarakis, S. L. Wang, M. Dorovkov, A. Ryazanov, M. Driscoll, *Nat. Genet.* **24**, 180 (2000).
15. M. E. Greenberg *et al.*, *J. Exp. Med.* **203**, 2613 (2006).
16. H. Bayir *et al.*, *Biochim. Biophys. Acta* **1757**, 648 (2006).
17. X. Wang *et al.*, *Science* **302**, 1563 (2003).
18. Z. Zhou, E. Hartwieg, H. R. Horvitz, *Cell* **104**, 43 (2001).
19. J. Yuan, S. Shaham, S. Ledoux, H. M. Ellis, H. R. Horvitz, *Cell* **75**, 641 (1993).
20. P. W. Reddien, S. Cameron, H. R. Horvitz, *Nature* **412**, 198 (2001).
21. D. J. Hoeppner, M. O. Hengartner, R. Schnabel, *Nature* **412**, 202 (2001).
22. T. Pomorski, A. K. Menon, *Cell. Mol. Life Sci.* **63**, 2908 (2006).
23. J. Ding *et al.*, *J. Biol. Chem.* **275**, 23378 (2000).
24. K. Balasubramanian, A. J. Schroit, *Annu. Rev. Physiol.* **65**, 701 (2003).
25. W. G. Kelly, S. Xu, M. K. Montgomery, A. Fire, *Genetics* **146**, 227 (1997).

26. We thank Y. Shi for help with constructs, A. Fire for the *ccIs4251* strain, J. Hutton for the *inIs179* strain, M. Hengartner for the *opIs117* strain, M. Driscoll for the *bzIs8* strain and the $P_{mec\text{-}4}$mCherry construct, and X. Xie and T. Blumenthal for comments on the manuscript. This work was supported by the Burroughs Wellcome Fund Career Award (D.X.), a grant from MEXT of Japan (S.M.), NIH grant R01 GM59083 (D.X.), and Human Frontier Science Program grant RGP0016/2005-C (D.X.).

Supporting Online Material

www.sciencemag.org/cgi/content/full/320/5875/528/DC1
Materials and Methods
SOM Text
Figs. S1 to S7
Tables S1 and S2
References and Notes

29 January 2008; accepted 11 March 2008
10.1126/science.1155847

Vaccinia Virus Uses Macropinocytosis and Apoptotic Mimicry to Enter Host Cells

Jason Mercer and Ari Helenius*

Viruses employ many different strategies to enter host cells. Vaccinia virus, a prototype poxvirus, enters cells in a pH-dependent fashion. Live cell imaging showed that fluorescent virus particles associated with and moved along filopodia to the cell body, where they were internalized after inducing the extrusion of large transient membrane blebs. p21-activated kinase 1 (PAK1) was activated by the virus, and the endocytic process had the general characteristics of macropinocytosis. The induction of blebs, the endocytic event, and infection were all critically dependent on the presence of exposed phosphatidylserine in the viral membrane, which suggests that vaccinia virus uses apoptotic mimicry to enter cells.

Poxviruses are enveloped DNA viruses that differ from other animal viruses in their large size and complexity (*1*). For humans, the most dangerous is variola virus, the causative agent of smallpox and one of most devastating pathogens in history. The development of new antiviral strategies against poxviruses will require detailed information about their replication cycle (*2*).

During replication, two infectious forms of vaccinia are produced: intracellular mature virus (MV) and extracellular enveloped virus (EV). The binding of MVs to cells involves cell-surface glycosaminoglycans (*3*), and MVs have been observed binding to actin-containing fingerlike protrusions (*4*). The viral envelope can fuse directly with the plasma membrane (*3*), but productive entry occurs mainly by low pH–dependent endocytosis into large uncoated vacuoles (*5*).

To follow the entry of individual virions, we generated MVs with an enhanced yellow fluorescent protein (EYFP)–tagged core protein [EYFP-CORE-MVs (*6*)]. When added to cells expressing enhanced green fluorescent protein (EGFP)–actin or enhanced cyan fluorescent protein–actin, virions that bound to filopodia moved toward the cell body (Fig. 1A and movies S1 to S3). As seen with other viruses (*7*), the movement was uninterrupted, with a rate approximating that of actin retrograde flow (1.05 ± 0.38 μm/min, fig. S1).

When MVs reached the cell body, a dramatic change occurred in the plasma membrane: A large, roughly spherical bleb (diameter 2 ± 0.57 μm; n = 42 blebs) extruded at the site of contact with the virus, followed by the formation of further blebs along the cell body. Each bleb remained extended for 10 ± 2 s (n = 42) before actin accumulated on the membrane, and the bleb retracted within 18 ± 3 s (n = 42) (Fig. 1B, movies S4 to S6, and figs. S2 and S3). Bleb retraction and cortical actin reassembly coincided with virus entry. Blebbing peaked 30 min after virus addition (Fig. 1C). The fraction of blebbing cells increased with the multiplicity of infection (MOI), while the number of blebs per blebbing cell remained in the range of 75 to 125 (Fig. 1, D and E, and fig. S4). Thus, a single incoming MV induced a generalized state in the cell that promoted bleb formation along the entire cell body.

To test whether blebbing was needed for infection, we used blebbistatin, an inhibitor of myosin II–dependent blebbing (*8*). Infection was quantified with EGFP-expressing MVs (EGFP-EXPRESS-MVs) and fluorescence-activated cell sorting (FACS) (fig. S5) (*6*). Blebbistatin prevented the formation of MV-induced blebs (fig. S6) and inhibited infection by 65% (Fig. 1F), which suggests that bleb formation was involved in productive entry.

In addition to actin, blebs contained Rac1, RhoA, ezrin, and cortactin (Fig. 1G), which are important for plasma membrane blebbing under other conditions (*9*) and for MV entry (*4*). MV-

ETH Zurich, Institute of Biochemistry, Schafmattstrasse 18, ETH Hönggerberg HPM E6.3 Zurich, Switzerland.

*To whom correspondence should be addressed. E-mail: ari.helenius@bc.biol.ethz.ch

Supporting Online Material for

Role of *C. elegans* TAT-1 Protein in Maintaining Plasma Membrane Phosphatidylserine Asymmetry

Monica Darland-Ransom, Xiaochen Wang, Chun-Ling Sun, James Mapes, Keiko Gengyo-Ando, Shohei Mitani, Ding Xue*

*To whom correspondence should be addressed. E-mail: ding.xue@colorado.edu

Published 25 April 2008, *Science* **320**, 528 (2008)
DOI: 10.1126/science.1155847

This PDF file includes:

Materials and Methods

Strains

C. elegans strains were maintained using standard methods *(S1)*. All alleles used for this study have been described in detail previously *(S2)*, except for the four integrated transgenes, *inIs179* (LGII), *ccIs4251* (LGI), *smIs76* (LGV), and *bzIs8* (LGX)*(S3-S5)*, and two *tat* deletion alleles, *tat-1(tm1034)* (LGIII) and *tat-3(tm1275)* (LGIII), which are described in detail below. *smIs142* is a spontaneous integration line derived from *tat-1(tm1034); bzIs8* transgenic animals carrying $P_{tat\text{-}1}$*tat-1::flag*.

The *C. elegans tat* genes

C. elegans tat genes are defined by six different open reading frames, Y49E10.11 (*tat-1*), H06H21.10 (*tat-2*), W09D10.2 (*tat-3*), T24H7.5 (*tat-4*), F36H2.1 (*tat-5*), and F02C9.3 (*tat-6*), and share 48%, 48%, 39%, 39%, 36%, and 36% sequence identity to a human aminophospholipid translocase, ATP8A1 *(S6, S7)*.

RNAi experiments

RNAi constructs from a *C. elegans* RNAi library (constructed by the Ahringer laboratory) were used to reduce the expression of the *tat-2, tat-3, tat-4, tat-5,* and *tat-6* gene *(S8)*. The *tat-1* RNAi construct was made by polymerase chain reaction (PCR) amplification of 310 bp of the *tat-1* coding region and then subcloning the PCR fragment into the RNAi vector pPD129.36 via its Nhe I and Xho I sites. All RNAi experiments were carried out using a bacterial feeding protocol *(S9)*. In most cases, wild-type animals were treated with RNAi for two generations before their progeny were assayed for

annexin V staining, except for the *tat-5* RNAi experiment, which causes lethality and progeny were examined for PS staining after only one round of RNAi treatment.

Isolation of the *tat-1(tm1034)* and *tat-3(tm1275)* deletion alleles

The *tat-1(tm1034)* and *tat-3(tm1275)* deletion alleles were isolated from TMP/UV mutagenized worms *(S10).* Nested PCR primers used to screen for the *tat-1(tm1034)* allele are 5' CTACACTGGACACGACTCAA 3' and 5' CCAGTATGACAAACAGCC-AT 3' for the first round amplification and 5' ACGACTCAAAGCTGCTCATG 3' and 5' CACATTCCGTGTAAGAGTGC 3' for the second round amplification. *tat-3(tm1275)* was screened using primers 5' CTCATTATGGGTACCCCCGA 3' and 5' CGGACGAC-CTCCATAGTCAT 3' for the first round amplification and 5' ACTGAGCATCGGCGG-AATAC 3' and 5' GTACCCCCGACACGGTAATT 3' for the second round amplification. Both mutants were backcrossed with wild-type (N2) animals at least 4 times before they were analyzed further.

Phosphatidylserine staining in adult gonads

Phosphatidylserine staining was performed on exposed adult gonads of wild-type animals, *tat* mutant animals, and *tat* RNAi-treated animals as described previously *(S11).* Briefly, gonads were gently dissected out from 24-48 hour old adult hermaphrodite animals by cutting them at the head in a depression slide while immersed in a gonad dissection buffer (60 mM NaCl, 32 mM KCl, 3 mM Na_2HPO_4, 2 mM $MgCl_2$, 20 mM HEPES, 50 μg/ml penicillin, 50 μg/ml streptomycin, 100 μg/ml neomycin, 10 mM Glucose, 33% fetal calf serum, and 2 mM $CaCl_2$). The exposed gonads were then washed

once in the dissection buffer and transferred to a dissection buffer containing 1 μl of Alexa Fluor 488-conjugated annexin V (Molecular Probes), 25 μM of propidium iodide, and 4 μM of Hoechst 33342. Gonads were washed one more time in the dissection buffer, placed on a 5% agarose pad, and visualized using a Nomarski microscope equipped with an epifluorescence detector.

Quantification of cell corpses

The number of somatic cell corpses in the head region of live embryos or L1 larvae and the number of germ cell corpses in one gonad arm from animals at various adult ages were scored using Nomarski optics, as previously described *(S11)*.

Quantification of missing cells

Several integrated transgenes carrying various GFP reporters were used to identify specific neurons, muscle cells, and other cell types in N2 or various mutant animals, which were scored using a fluorescent Nomarski microscope. In most experiments, L4 larvae were examined for the presence of GFP-labeled cells, except for *ccIs4251* animals, which were scored at the L1 larval stage.

Molecular Biology

Full-length *tat-1* cDNA clone was constructed from two partial *tat-1* cDNA clones, *yk423h8* and *yk1018h06* (gifts from Dr. Yuji Kohara). $P_{tat\text{-}1}$*tat-1::flag* was constructed by ligating a 2.8 kb *tat-1* genomic fragment containing 2.4 kb of the promoter sequence and the first two exons and the first intron to a 3.35 kb *tat-1* cDNA fragment starting from an

internal Sph I site in the second exon and ending with its carboxyl terminus tagged with a FLAG epitope (DYKDDDDK). This *tat-1::flag* minigene fully rescued the missing cell phenotype of the *tat-1(tm1034)* mutant. The *tat-1* inverted repeat (IR) RNAi construct (P_{mec-7}*tat-1IR*) was generated through three-piece ligation among two identical 701 bp BspHI-Sph I *tat-1* cDNA fragments derived from the pSL1190-*tat-1* cDNA clone and the pPD52.102 (P_{mec-7}) vector backbone previously digested with Nco I, yielding a 1.4 kb insert containing inverted repeat *tat-1* cDNA fragments under the control of the *mec-7* promoter.

Assays for PS externalization in PLM cells and PLM cell loss

P_{mec-7}*tat-1IR* (25 μg/ml) or P_{mec-7}vector (25 μg/ml) was co-injected with P_{mec-4}mCherry (25 μg/ml) into N2 animals carrying an integrated transgene (*smIs76*) that contains P_{hsp}ANV::GFP using pRF4 (50 μg/ml) as a co-injection marker. Transgenic animals were synchronized as embryos and allowed to age 18 hours. The animals were then subjected to the following heat-shock treatment: 16˚C for 10 minutes, 30˚C for 35 minutes and allowed to recover for 2 hours at 16˚C before they were scored for surface PS exposure in the PLM cells at the L2 larval stage using 100 mM levamisole. Missing PLM cells were scored in the L4 larval stage transgenic animals based on the expression of mCherry in the PLM cells.

Heat-shock treatment of *opIs117* animals

Hermaphrodite animals 48 hours after the L4/Adult molt were subjected to the heat-shock treatment at 33°C for 30 minutes and allowed to recover for 6 hours as previously

described (*S12*). Animals were then subjected to epifluorescence and DIC microscopy and assayed for PS exposure on the surface of germ cells.

Antibody Staining

Gonads were dissected out of hermaphrodite animals as described above, fixed with methanol, and rehydrated with phosphate buffered saline (PBS, pH8.0). The gonads were then stained with anti-FLAG antibody (M2, Sigma), which was preabsorbed with acetone powder made from the *tat-1(tm1034)* worm lysate at room temperature for 1 hour. Following anti-FLAG antibody staining, gonads were washed four times with PBS (pH6.0) and then stained with FITC-conjugated goat anti-mouse antibody (Vector Laboratories Inc.), which was also preabsorbed with acetone powder made from the *tat-1(tm1034)* worm lysate, and 10 μg/ml of DAPI in PBS (pH8.0) at room temperature for 1 hour. After that, gonads were washed with PBS (pH6.0) as before, mounted on slides, and visualized using a Nomarski microscope equipped with a fluorescence detector.

Supporting Online Text

Ectopic PS exposure in germ cells of *tat-1* deficient animals is not due to the activation of a *C. elegans* phospholipid scramblase or WAH-1

We tested the possibility that loss of *tat-1* might activate a lipid flipping enzyme that promotes PS exposure, such as the *C. elegans* phospholipid scramblase SCRM-1, or the

SCRM-1 activator, WAH-1 [worm apoptosis-inducing factor (AIF) homologue], both of which promote externalization of PS in apoptotic germ cells *(S11).* Germ cell staining of PS was not reduced in the *scrm-1(tm698); tat-1(tm1034)* double mutant or in *tat-1(tm1034)* animals treated with *wah-1(*RNAi), compared with that in the *tat-1(tm1034)* mutant alone or in *tat-1(tm1034)* animals treated with control RNAi (Fig. S2, A and B). Similar amounts of germ cell PS staining were observed in *scrm-4(tm624) scrm-2(tm650); scrm-3(tm631)* triple mutant animals treated with *tat-1*(RNAi) to that seen in wild-type animals treated with *tat-1*(RNAi) (Fig. S2C). Thus, loss of SCRM-1, WAH-1, or other *C. elegans* phospholipid scramblases does not affect PS externalization in *tat-1* deficient animals, although we cannot exclude the possibility that TAT-1 may act by negatively regulating another phospholipid translocating enzyme.

Comparison of two different *C. elegans* PS staining protocols and results derived from the use of these two protocols

A previous study using an integrated transgene (*opIs117*) expressing a secreted form of a fusion protein containing green fluorescent protein and annexin V (GFP::AnxV) as a PS sensor reached the opposite conclusion that *tat-1* promotes externalization of PS in *C. elegans* apoptotic cells *(S12),* since staining of germ cell corpses by GFP::AnxV decreased in *tat-1(RNAi)* animals. We think that the difference between the two studies could result from the relatively weak binding of GFP::AnxV *in vivo* to surface-exposed PS and a high staining background (Fig. S3A). A high amount of background staining may have prevented detection of weak surface PS exposure in *tat-1(RNAi)* animals (Fig. 1B and Fig. S3A)*(13).* In addition, widespread exposure of PS in all germ cells of *tat-*

1(RNAi) animals may have competed for the binding of GFP::AnxV and caused reduction of PS staining in apoptotic germ cells.

The Alexa Fluor 488-conjugated annexin V that we used binds strongly and specifically to surface exposed PS and we optimized the staining ex vivo on dissected gonads *(S11, S13)*. We observed staining of PS in all germ cells of *ced-1(e1735); tat-1(tm1034)* animals and no reduction in PS staining of apoptotic germ cells compared with that in *ced-1(e1735)* animals (Fig. S4), which are defective in cell corpse engulfment and allow scoring of more germ cell corpses, indicating that PS exposure in apoptotic germ cells is not affected by the loss of the *tat-1* gene. In a *tat-1(tm1034); opIs117* strain, the ex vivo PS staining protocol stained all germ cells of these animals, whereas GFP::AnxV labeling of normal germ cells was not seen in these animals when we applied the protocol used by Zullig et al. (Fig. S3B)*(S12)*.

Figure S1A

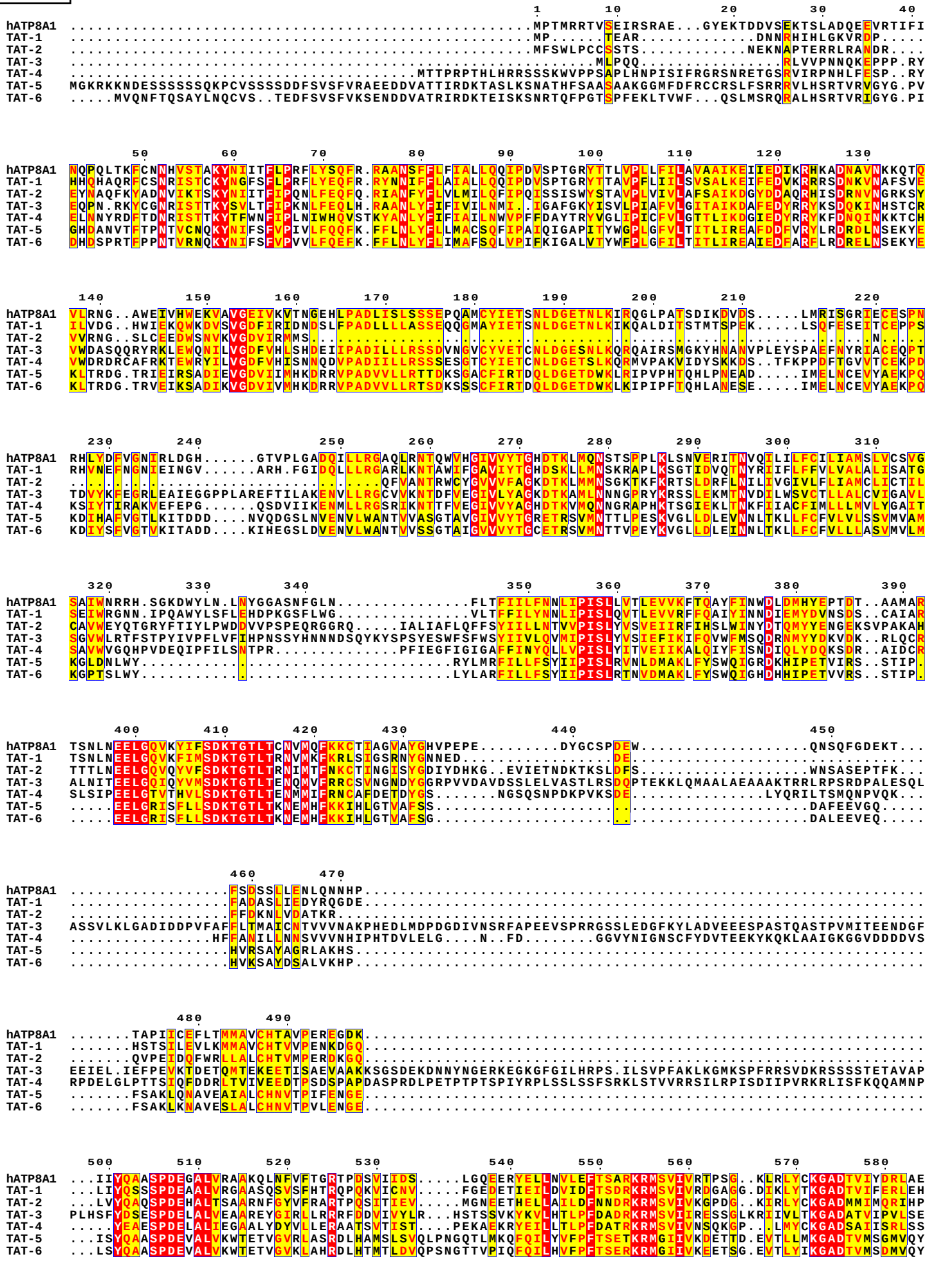

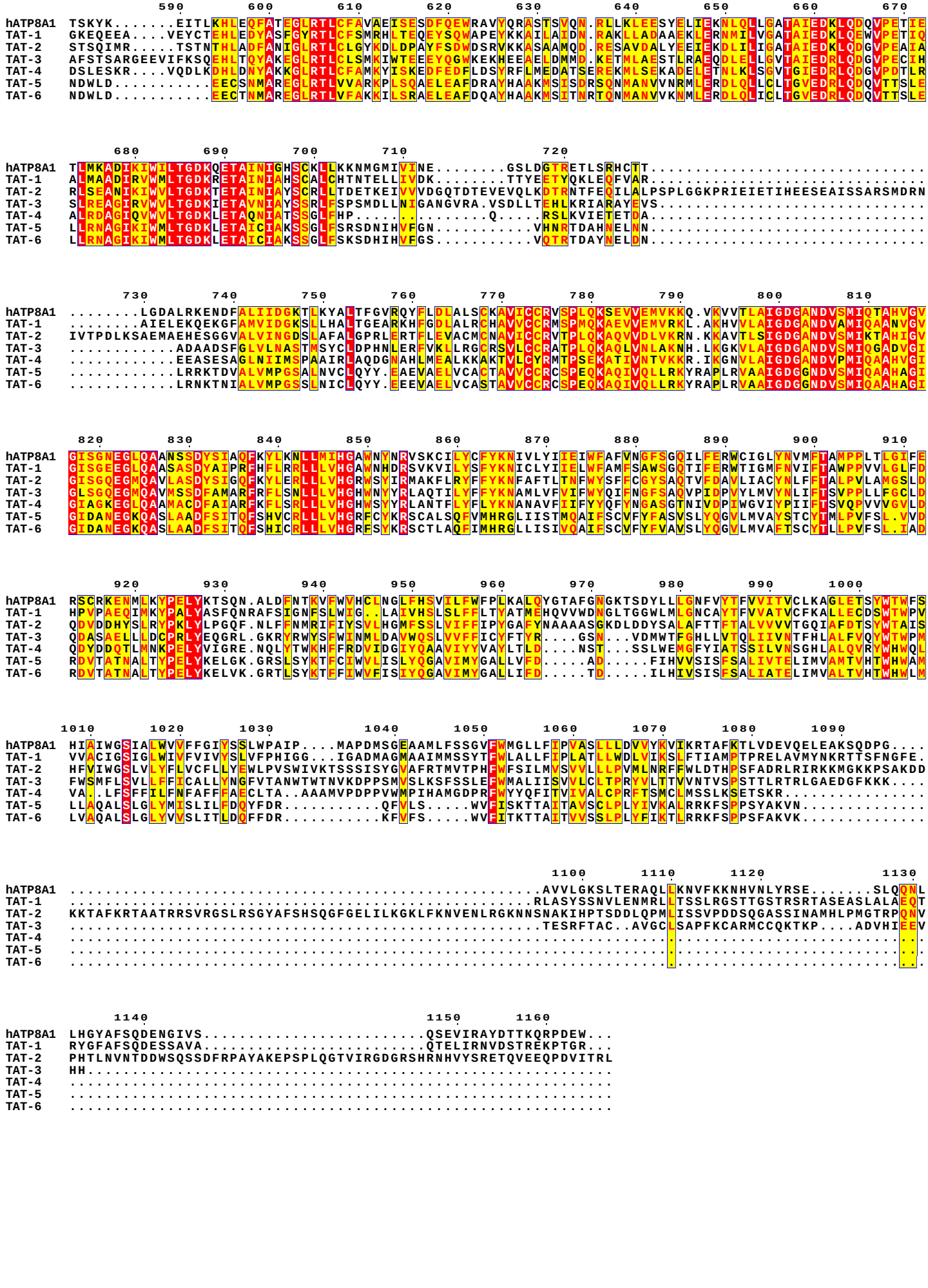

B.

tat-1(tm1034)

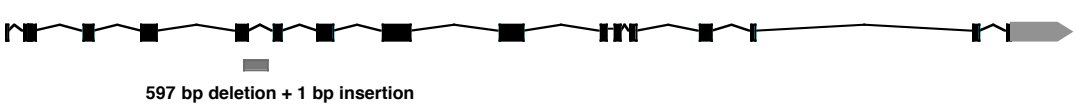

597 bp deletion + 1 bp insertion

tat-3(tm1275)

446 bp deletion + 7 bp insertion

Figure S1. The *tat* protein sequences and deletion alleles. **(A)** Sequence alignment of all 6 *C. elegans* TAT proteins with human ATP8A1. Residues that are identical are shaded in red, residues that are similar are shaded in yellow**. (B)** The *tat-1* and *tat-3* deletion alleles. Black boxes indicate exons of *tat-1* and *tat-3* genes. Wave lines indicate introns of these two genes. The region deleted in each gene is indicated with a gray box underneath the gene.

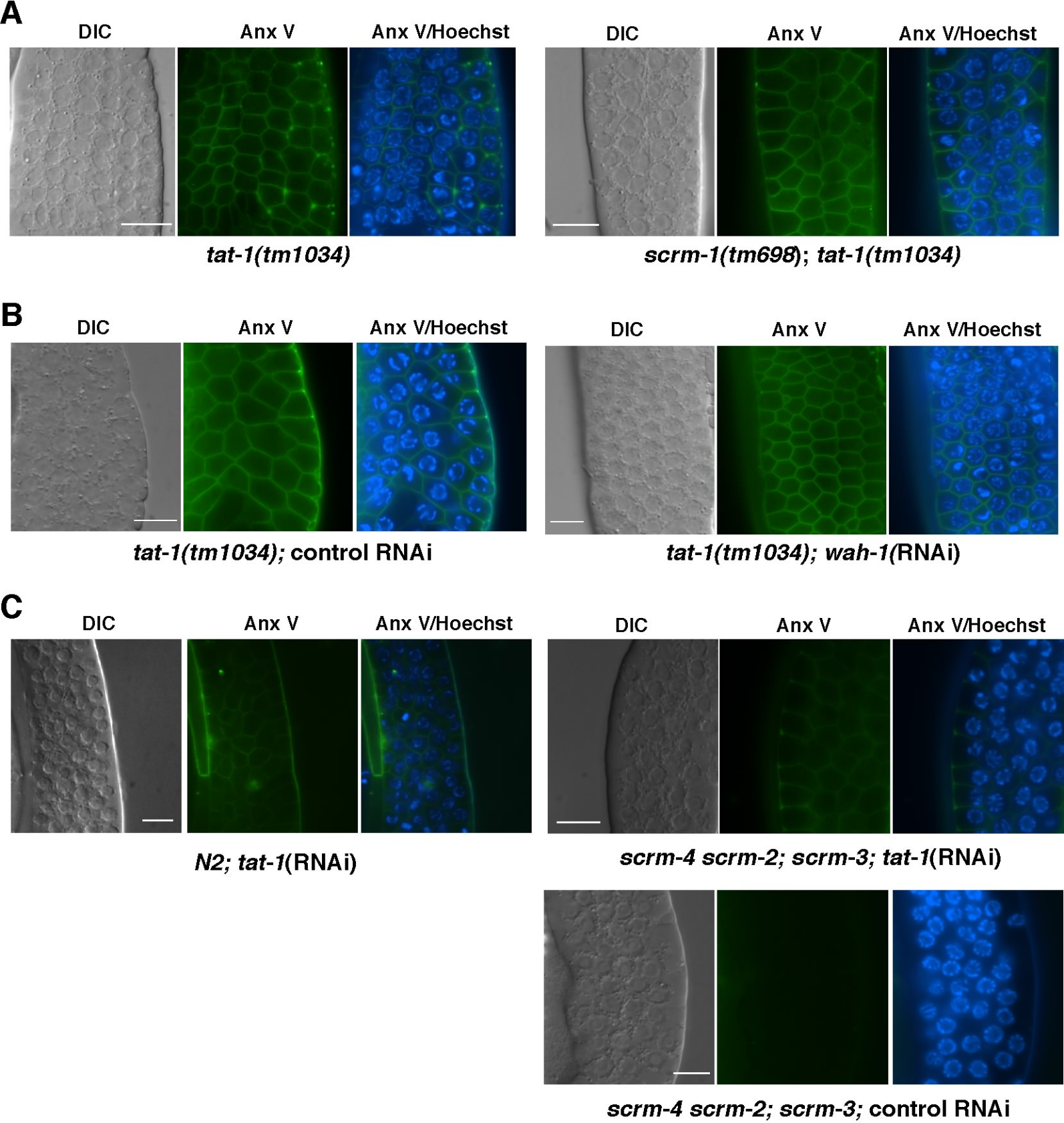

Figure S2. PS externalization in germ cells of *tat-1(tm1034)* animals is not affected by the loss of *C. elegans* phospholipid scramblases. Exposed gonads from the following adult hermaphrodite animals were stained with Annexin V as described in Figure 1: (**A**) *tat-1(tm1034)* and *scrm-1(tm698); tat-1(tm1034)* animals, (**B**) *tat-1(tm1034);* control RNAi and *tat-1(tm1034); wah-1*(RNAi) animals, (**C**) wild-type animals (N2) treated with *tat-1*(RNAi), *scrm-4(tm624) scrm-2(tm650); scrm-3(tm631); tat-1*(RNAi) animals, and *scrm-4(tm624) scrm-2(tm650); scrm-3(tm631);* control RNAi animals. All *scrm* mutations used are strong loss-of-function or null mutations *(S11)*. The PS exposure phenotype caused by *tat-1*(RNAi) is weaker than that caused by the *tat-1(tm1034)* mutation. Images of DIC, Annexin V staining, and the merged image of Annexin V+ Hoechst 33342 staining are shown. Scale bars indicate 6.5 μM.

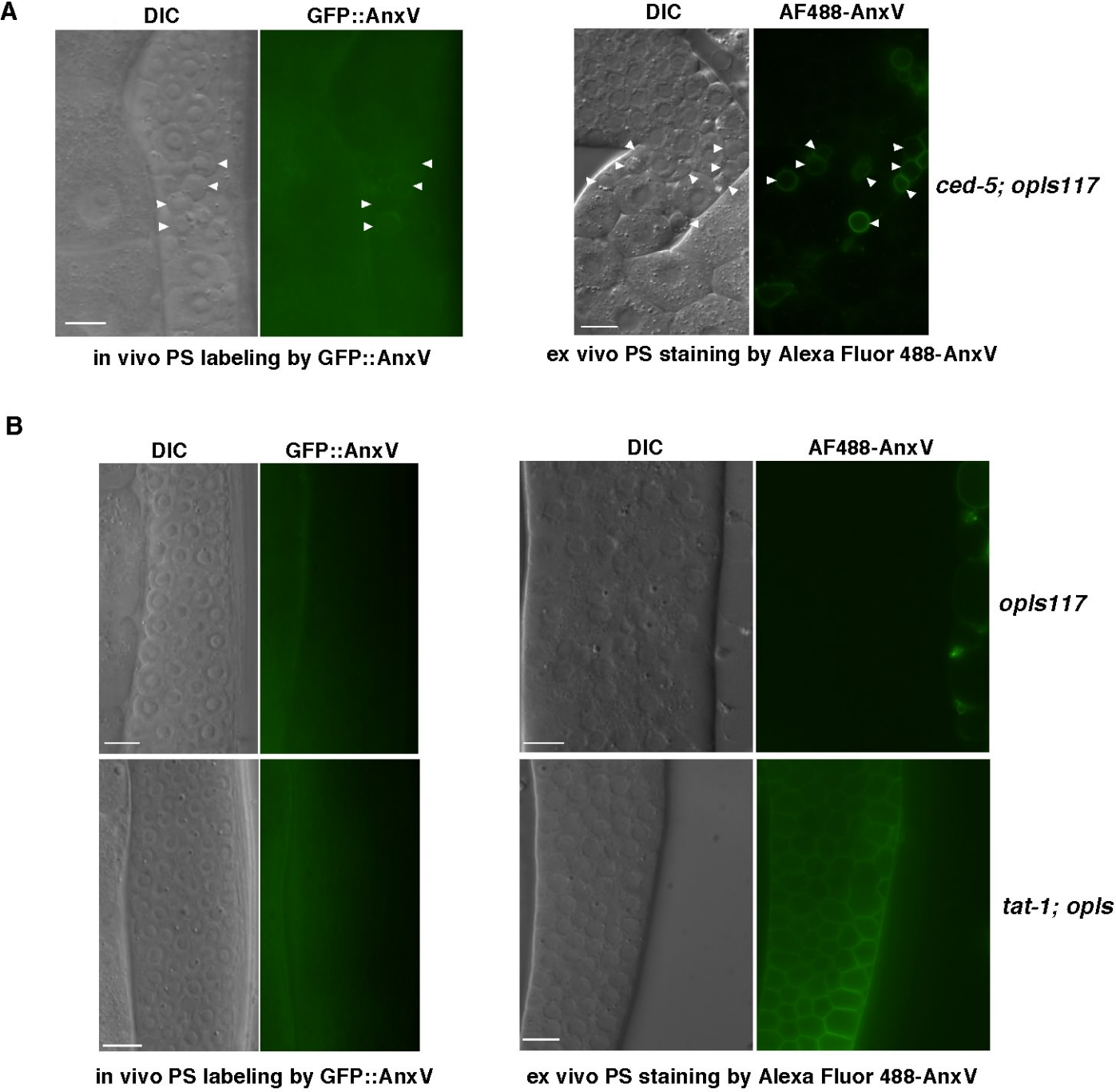

Figure S3. Comparison of ex vivo PS staining on dissected gonads using Alexa Fluor 488 conjugated Annexin V (AF488-AnxV) with in vivo PS labeling using a secreted form of GFP annexin V fusion (GFP::AnxV). The ex vivo PS staining and in vivo PS labeling experiments were carried out as described in Materials and Methods. (**A**) The ex vivo PS staining protocol results in stronger PS staining on germ cell corpses and less background staining than the in vivo PS labeling protocol. *ced-5(n1812); opIs117* animals were stained or labeled. Germ cell corpses are indicated with white arrowheads. Images of DIC and GFP::AnxV or AF488-AnxV are shown. Not all germ cell corpses were labeled by GFP::AnxV or AF488-AnxV. For example, approximately 75% germ cell corpses in *ced-5(n1812)* animals were labeled by AF488-AnxV (*S11*). In addition, some apoptotic germ cells labeled by GFP::AnxV or AF488-AnxV had not yet displayed an obvious cell corpse morphology. **(B)** The ex vivo PS staining protocol but not the in vivo PS labeling protocol reveals surface PS exposure in all germ cells in *tat-1(tm1034); opIs117* animals. *opIs117* and *tat-1(tm1034); opIs117* animals were stained or labeled. Scale bars indicate 6.5 μM.

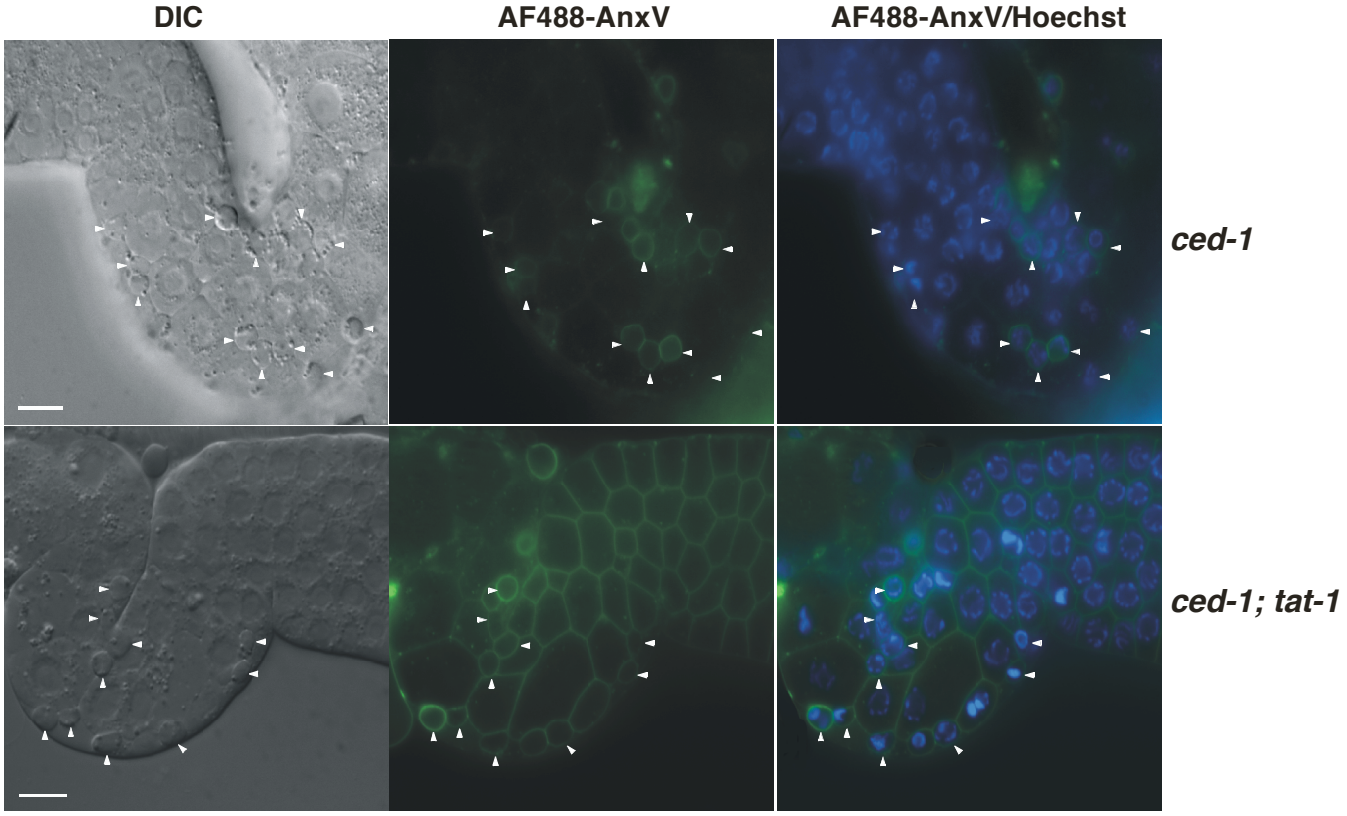

Figure S4. Inactivation of the *tat-1* gene does not affect PS externalization in apoptotic germ cells. Gonads of *ced-1(e1735)* or *ced-1(e1735); tat-1(tm1034)* animals were dissected out and stained ex vivo with Alexa Fluor 488 conjugated Annexin V (AF488-AnxV) as described in Materials and Methods. Images of DIC, AF488-AnxV, and merged image of AF488-AnxV/Hoescht 33342 are shown. Germ cell corpses, which display raised-button-like morphology under Nomarski optics, are indicated by white arrowheads. As described previously (*S11*), approximately 60% germ cell corpses in *ced-1(e1735)* animals are stained by AF488-AnxV. In *ced-1(e1735)* animals, only germ cell corpses were stained by AF488-AnxV. In *ced-1(e1735); tat-1(tm1034)* animals, both apoptotic and normal germ cells were stained. Scale bar indicates 6.5 μM.

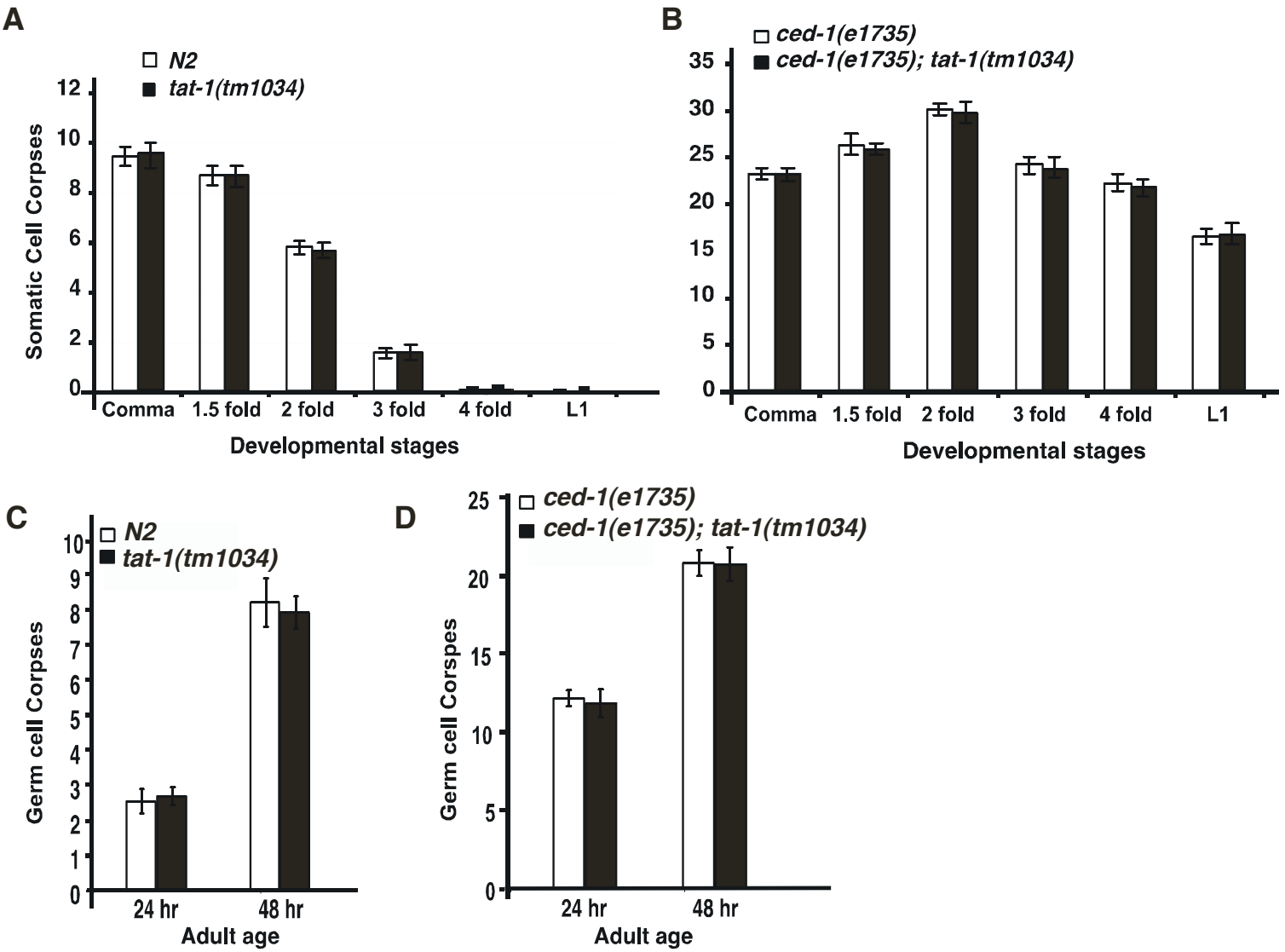

Figure S5. The *tat-1(tm1034)* mutation does not affect cell death or removal of apoptotic cell corpses in the soma or in the germline. **(A, B)** Embryonic cell corpse profiles of N2 (wild-type), *tat-1(tm1034), ced-1(e1735),* and *ced-1(e1735); tat-1(tm1034)* embryos and L1 larvae. The numbers of somatic cell corpses were scored at the following embryonic or larval stages: bean or comma (comma), 1.5-fold, 2-fold, 3-fold, 4-fold, and early L1 larvae (L1). The *y* axis indicates the average number of cell corpses counted in the head region of embryos or larvae. Error bars represent SEM. At least 15 animals were scored for each developmental stage. **(C, D)** Germ cell corpse profiles of N2, *tat-1(tm1034), ced-1(e1735),* and *ced-1(e1735); tat-1(tm1034)* animals. The numbers of germ cell corpses were scored 24 hours and 48 hours after the L4 to adult molt from one gonad arm of the animals. The *y* axis indicates the average number of germ cell corpses. Error bars represent SEM. At least 15 animals were scored for each time point.

A

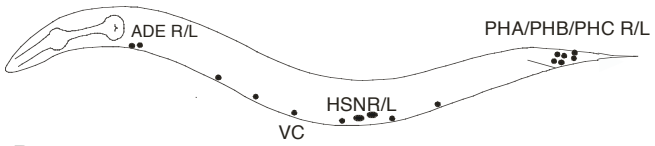

B

Strain	% animals missing at least one labeled neuron
inIs179	**1%**
inIs179; tat-1(tm1034)	**24%**
inIs179; tat-3(tm1275)	**2%**
inIs179; psr-1(tm469)	**2%**
inIs179; tat-1(tm1034); psr-1(tm469)	**2%**
ced-1(e1735); inIs179	**2%**
ced-1(e1735); inIs179; tat-1(tm1034)	**1%**

Fig. S6. Loss of neurons in *tat-1* deficient animals through a mechanism mediated by *psr-1* and *ced-1*. An integrated GFP reporter line, *inIs179*, labels a variety of neurons in the head, the body, and the tail (**A**). Neurons scored are indicated with black circles. The presence of various neurons was scored using a Nomarski microscope with epifluorescence (**B**). The percentages of animals missing one or more neurons are shown. >200 animals were scored for each strain.

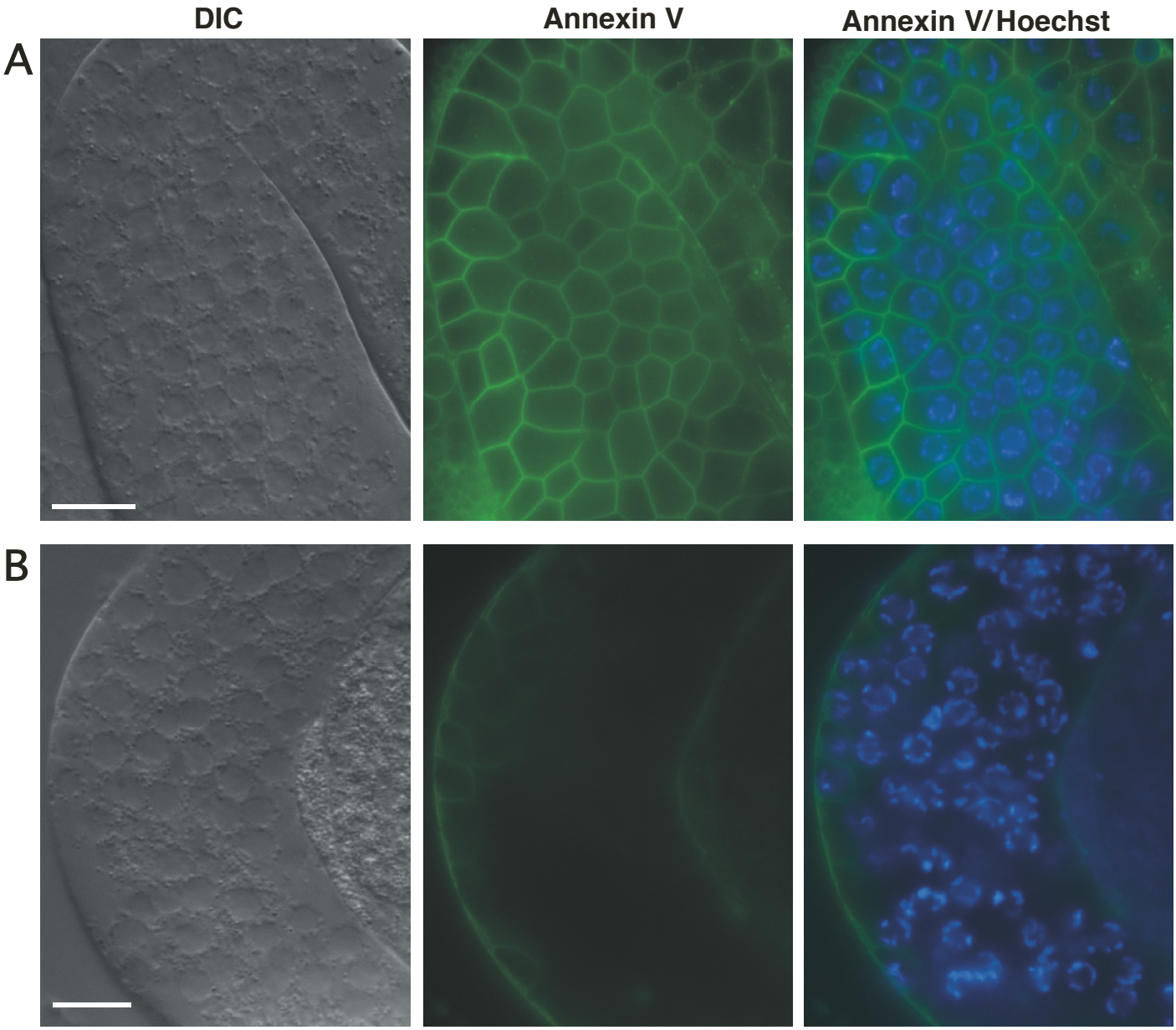

Figure S7. A TAT-1::FLAG minigene can rescue the germ cell PS exposure phenotype of the *tat-1(tm1034)* mutant. Exposed gonads of the following hermaphrodite adult animals were stained with Annexin V as described previously *(S11).* (**A**) *tat-1(tm1034); bzIs8* animal and (**B**) *tat-1(tm1034); smIs142; bzIs8* animal. Images of DIC, Annexin V staining, and the merged image of Annexin V+ Hoechst 33342 staining are shown. Scale bars indicate 6.5 μM.

Table S1. RNAi treatment of the *C. elegans tat* genes and PS staining on RNAi-treated animals. RNAi experiments were conducted using a bacterial feeding protocol as described previously *(S9).* RNAi treated animals were stained with annexin V as described in Materials and Methods. All animals were treated with RNAi for two generations before the PS staining assays were performed, except for *tat-5*(RNAi) animals, which were lethal and were scored in the first generation of RNAi treatment.

Gene	PS staining on germ cells
tat-1	weak
tat-2	no
tat-3	no
tat-4	no
tat-5	no
tat-6	no

Table S2. Rescue of the missing cell phenotype of the *tat-1(tm1034)* mutant by various transgenes expressing the TAT-1::FLAG fusion protein. P_{tat-1}*tat-1::flag* (25 ng/μl) was injected into *tat-1(tm1034); bzIs8* animals with pRF4 as a co-injection marker (50 ng/μl). Three extrachromosomal transgene arrays (*smEx3617, smEx3618,* and *smEx3619)* and one spontaneous integrated transgene array (*smIs142*) were generated. The presence of six touch receptor neurons in transgenic animals was scored as described in Figure 2 using a fluorescent Nomarski microscope. The percentage of animals (n=200) missing at least one touch cell is shown**.**

Transgene	% of animals missing at least one touch receptor neuron
bzIs8	1
tat-1(tm1034); bzIs8	19
tat-1(tm1034); bzIs8; smEx3617	3
tat-1(tm1034); bzIs8; smEx3618	2
tat-1(tm1034); bzIs8; smEx3619	1
tat-1(tm1034); smIs142; bzIs8	1

References and Notes

S1. S. Brenner, *Genetics* **77**, 71 (1974).
S2. D. L. Riddle, T. Blumenthal, B. J. Meyer, J. R. Preiss, Eds., *C. elegans II* (Cold Spring Harbor Laboratory Press, Cold Spring Harbor, New York, 1997), pp.
S3. T. R. Zahn, M. A. Macmorris, W. Dong, R. Day, J. C. Hutton, *J. Comp. Neurol. 429*, **127** (2001).
S4. D. C. Royal *et al.*, *J. Biol. Chem.* **280**, 41976 (2005).
S5. L. Timmons, D. L. Court, A. Fire, *Gene* **263**, 103 (2001).
S6. M. E. Auland, B. D. Roufogalis, P. F. Devaux, A. Zachowski, *Proc. Natl. Acad, Sci. U S A* **91**, 10938 (1994).
S7. J. K. Paterson *et al.*, *Biochemistry* **45**, 5367 (2006).
S8. A. G. Fraser *et al.*, *Nature* **408**, 325 (2000).
S9. X. Wang, C. Yang, J. Chai, Y. Shi, D. Xue, *Science* **298**, 1587 (2002).
S10. K. Gengyo-Ando, S. Mitani, *Biochem. Biophys. Res. Commun.* **269**, 64 (2000).
S11. X. Wang *et al.*, *Nat. Cell Biol.* **9**, 541 (2007).
S12. S. Zullig *et al.*, *Curr. Biol.* **17**, 994 (2007).
S13. M. Darland, D. Xue, unpublished results (2008).